 CMES, vol.33, no.2, pp.131-153, 2008

Unsteady 3D Boundary Element Method for Oscillating Wing

Marco La Mantia[1] **and Peter Dabnichki**[1,2]

Abstract: A potential flow based boundary element method was devised to obtain the hydrodynamic forces acting on oscillating wings. A new formulation of the unsteady Kutta condition, postulating a finite pressure difference at the trailing edge of the flapping wing and proposed earlier by the authors, is implemented in the numerical procedure. A comparison with published experimental data (Read et al., 2003) is carried out and the three-dimensional computational results showed good agreement, especially if compared with a similar two-dimensional numerical approach (La Mantia and Dabnichki, 2008) and the potential analytical model of Garrick (1936). The need of considering the differences between the actual flow conditions and the assumptions of the computational model (e.g. to estimate inertia related effects) is underlined and the potential three-dimensional code is deemed to be a further step in the direction of a novel physically based modelling of flapping flight.

Keyword: Panel method, Unsteady flow, Flapping wing

1 Introduction

Birds have always fascinated humans with their ability to defy gravity and roam the vast air. Slightly later there a considerable interest was sparked into understanding the locomotion of different aquatic species. Only in the 20^{th} century humans started analysing their own ability to swim which lead to a considerable interest into the different mechanisms of human propulsion. Lauder and Dabnichki and Bartlett (2001) demonstrated the crucial role of an precise kinematic analysis for accurate estimate of a propulsion force in human front crawl swimming. Lauder and Dabnichki (2005) developed experimental simulation through the use of robotic arm that allowed direct measurement of the propulsive force and produced somewhat

[1] School of Engineering and Materials Science, Queen Mary, University of London, Mile End Road, London E1 4NS, United Kingdom
[2] Corresponding author. Email: p.dabnichki@qmul.ac.uk

unexpected results. Subsequently Gardano and Dabnichki (2006a, 2006b) produced a BEM based computational model that showed very close agreement with the above experimental results. The model proposed by Gardano and Dabnichki (2006a) showed that BEM is very well suited for unsteady analysis as it allows to separate the kinematic contribution and the dynamic effect y modelling the added mass effect. They also showed that the added mass effect is by far the most important contributor in human propulsion generation. However, the limitation of the proposed model is that it is in essence quasi-static and as such is not fully suited for analysis of aquatic species who use different propulsion modes. La Mantia and Dabnichki (2006, 2007) proposed a new approach to model the kinematics by implementing wake modelling. This approach has been further developed in the three dimensional case in this work.

The interest in the area of aquatic and aerial propulsion of animals is long standing and there is a wealth of theoretical and experimental results, a short over view of which is presented below. Rozhdestvensky and Ryzhov (2003) reviewed theoretical and experimental studies of flapping-wing propulsors and of vehicles equipped with them. The complex character of the problem was underlined and key areas of interest identified, e.g. the effects of flow unsteadiness, wing flexibility and three-dimensionality. Triantafyllou et al. (2004) described the progress in understanding some basic mechanisms of force production and flow manipulation in oscillating wings for underwater use. Their review, focused primarily on experimental studies, showed that there is a considerable gap in understanding of flapping flight mechanism.

A number of works (Anderson et al., 1998, Read et al., 2003, and Schouveiler et al., 2005) studied experimentally an aquatic propulsion system able to produce such large forces. Experiments on a harmonically heaving and pitching wing were performed to determine its propulsive efficiency, as a function of the principal parameters: (i) phase angle between the heave and pitch motions, (ii) heave amplitude, (iii) Strouhal number and (iv) maximum angle of attack. Systematic measurements showed the existence of an efficiency peak for optimal set of parameters. A parameters' range where adequate efficiency and high thrust are achieved together was also identified.

Basu and Hancock (1978) were among the first to develop a panel method for the calculation of the forces on a two-dimensional rigid foil undergoing an arbitrary unsteady motion in an inviscid and incompressible flow. An appropriate boundary condition, known as Kutta condition, was added to obtain a unique solution. It defines the flow characteristics at the trailing edge of the moving foil.

The steady two-dimensional trailing-edge condition was independently formulated by Chaplygin (1910), Kutta (1910) and Zhukovski (1910) to avoid the mathematical

difficulties of the conformal mapping method at the foil trailing edge. The condition ensures that the flow passes the trailing edge smoothly with a finite velocity. Hess (1990), in a broad review of various panel methods, stated that the specification of a proper Kutta condition is more important than any other detail of the numerical implementation.

Poling and Telionis (1986) examined a number of unsteady flowfields and their experimental results indicate that the classical Kutta condition, which states that the velocity at the trailing edge is finite and the pressure difference there is zero, is not valid in certain conditions. Other experimental studies (Satyanarayana and Davis, 1978, and Ho and Chen, 1981) reached similar conclusions analysing the flow in the proximity of the trailing edge of oscillating wings. McCroskey (1982), in a wide ranging review of unsteady aerodynamics, stated that finite pressure loading and abrupt streamlines curvature could exist in the trailing-edge region of oscillating wing. The numerical results of Young and Lai (2004) show that flow separation occurs at the trailing edge of heaving foils creating an effective blunt-edge body. More precisely, the flow streamlines form time-dependant trailing-edge vortices rather than smoothly departing from the trailing edge on both sides. The edge flow mechanism was independently analysed by Liebe (2007) who proposed to replace the classical Kutta condition with a more general condition based on the formation and periodic shedding of trailing-edge vortices. This led to the development of a novel approach (Finite Vortex Model) for computing the forces acting on fixed and moving wings.

There is not any experimental evidence supporting the notion that the pressure difference at the trailing edge for unsteady motion of high frequency and large amplitude ought to be equal to zero. Contrary to this, the works of Satyanarayana and Davis (1978), Ho and Chen (1981) and Poling and Telionis (1986) suggest that the pressure difference should be finite rather than zero. In essence the relaxation of the postulated zero pressure difference at trailing edge is a logical first step in the formulation of a comprehensive unsteady Kutta condition, as discussed by La Mantia and Dabnichki (2008). This would allow considering the variation in direction and magnitude of the velocities across the trailing edge (in essence to consider the formation and shedding of trailing-edge vortices). Such more general pressure condition also aims to account for the viscosity effects in the otherwise inviscid numerical model. A similar modified trailing-edge condition for unsteady flows was already employed in a two-dimensional potential boundary element method (La Mantia and Dabnichki, 2008) and its implementation in a three-dimensional panel method is presented here.

The boundary element method and the related panel method have been successfully applied to various fluid mechanics problems (Soares and Mansur, 2005, Gar-

dano and Dabnichki, 2006a, Sellountos and Sequeira, 2008, and Sellier, 2008) and showed both computational speed and reliability, especially if compared to other numerical methods such as large eddy simulation (LES) and direct numerical simulation (DNS).

The aim of the present work is to investigate the effect of finite pressure difference at the trailing edge on the lift and thrust generated in water by flapping wing and to compare the numerical results with experimental data (Read et al., 2003) and two-dimensional computational models (Garrick, 1936, and La Mantia and Dabnichki, 2008).

2 Computational Model

An unsteady boundary element method computer program was developed to estimate the hydrodynamic forces on oscillating wing. A NACA 0012 symmetric wing was used similarly to the experiments by Anderson et al. (1998), Read et at. (2003), and Schouveiler et al. (2005). For such a wing of chord c and span s, moving forward at an average, steady velocity Q_∞, oscillating harmonically with a heave motion $z(t)$ transversely to the velocity Q_∞ and with a pitch motion $\gamma(t)$, which is also the instantaneous angle between Q_∞ and the chord, the following kinematic equations hold

$$z(t) = z_0 \sin(\omega t) \tag{1}$$

$$\gamma(t) = \gamma_0 \sin(\omega t + \psi), \tag{2}$$

where ψ is the phase angle between the heave and pitch motions, z_0 the heave amplitude, γ_0 the pitch amplitude and ω the frequency of oscillation (in radians per second). The pitch axis x_{pitch}, which is parallel to the leading and trailing edges of the wing, was set at one third of the chord. The instantaneous angle of attack $\alpha(t)$ is defined as

$$\alpha(t) = \gamma(t) - \tan^{-1}\left[\frac{\dot{z}(t)}{Q_\infty}\right], \tag{3}$$

where $\dot{z}(t)$ is the heave velocity.

The essential parameters for the solution of the problem are the phase angle ψ, heave amplitude z_0, Strouhal number St and maximum angle of attack α_{max}. The phase difference between the heave and pitch motions was set to 90 degrees, which corresponds to the optimum propulsion (Read et at, 2003, and Schouveiler et al., 2005). The heave amplitude was posed equal to three quarter of the foil chord. The Strouhal number, which is proportional to the maximum slope of the path, can be considered a measure of the degree of non-linearity of the motion. It indicates

how often vortices are created in the wing wake and how close they are. It is mathematically expressed by using the product of the frequency of vortex formation behind the wing (in Hz) and the width of the wake (assumed equal to two times the heave amplitude), divided by the flow main speed, i.e.

$$St = \frac{\omega}{2\pi}\frac{2z_0}{Q_\infty} = \frac{\omega z_0}{\pi Q_\infty}. \tag{4}$$

If Q_∞, z_0 and St are fixed, it is then possible to compute the frequency of oscillation ω. The definition of the instantaneous angle of attack, i.e. Equation (3), can now be rewritten as

$$\alpha(t) = \gamma_o \cos(\omega t) - \tan^{-1}[\pi St \cos(\omega t)]. \tag{5}$$

The instantaneous angle of attack is not explicitly related to the initial conditions. In general, for each Strouhal number St, when the maximum of the angle of attack α_{max} is fixed, there are a number of possible pitch amplitudes, that is, possible angle of attack time paths. More precisely, by using an iterative procedure that involves the time-derivative of Equation (5), the angle of attack time paths in which the fixed α_{max} is a global maximum can be evaluated. Besides, it is important to note that there are not closed-form solutions for particular combinations of St and α_{max}.

A number of kinematic parameters of the investigated motion are illustrated in Figures 1 and 2.

Figure 3 displays the instantaneous angle of attack as a function of St and time for α_{max}=15 deg. It is interesting to note that, if the Strouhal number is larger than 0.3, the initial angle of attack is generally lower than the maximum one.

Following Katz and Plotkin (2001), the flow is assumed incompressible and irrotational. Each wing section is represented by a finite number N of linear panels. The wing is divided into N_S strips, i.e., the wing is geometrically approximate by using N_S+1 sections perpendicular to the span. The wing is then modelled by using $N * N_S$ quadrilateral panels. Constant strength distributions of source σ and doublet μ are situated on each panel, the midpoint of which is called collocation point. The flow potential function $\phi*$ at each collocation point is defined as the sum of a local (perturbation) potential ϕ, related to the unknown doublet strength, and a free-stream potential ϕ_∞, linked to the fluid kinematic velocity. An internal Dirichlet boundary condition is imposed, that is, an inner potential function is specified on the internal wing surface in order to meet the non-penetration condition. At each wing collocation point the source strength is known, $\sigma = \bar{n}q_k$, where $\bar{n}$ is a unit vector normal to the wing surface pointing into the body and q_k the fluid kinematic velocity due to the motion of the wing. The governing integral equation is derived by using the

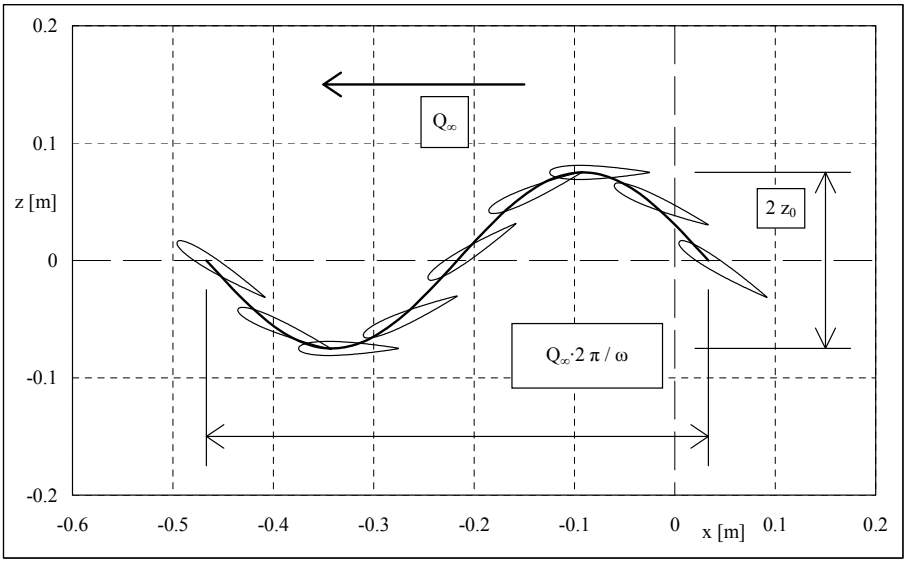

Figure 1: Kinematic parameters of the wing motion: c=0.1 m, s=0.6 m, x_{pitch}=0.033 m, Q_∞=0.4 m/s, z_0=0.075 m, St=0.3, ψ=90 deg, α_{max}=15 deg and γ_0=28.304 deg. Besides, the wing path is shown in the (x, z) plane of the inertia frame of reference, that is, the plane perpendicular to the span.

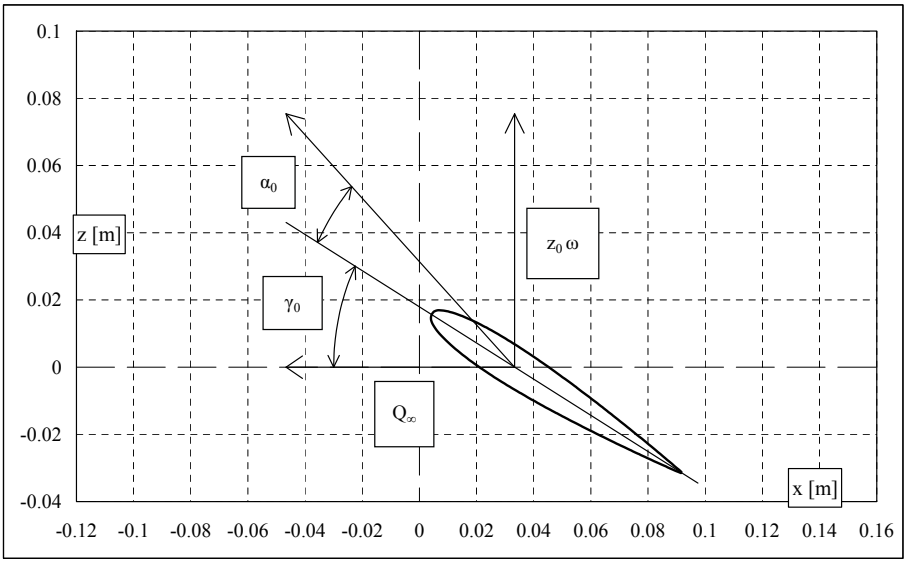

Figure 2: The initial kinematic angles of the oscillating wing. The motion parameters are the same used in Figure 1. In this case, according to Equation (3), the pitch amplitude γ_0 is assumed positive and the initial angle of attack α_0 is then negative, and equal to -15 deg. Besides, the frequency of oscillation ω is equal to 5.027 rad/s, i.e. $\omega/2\pi$=0.8 Hz.

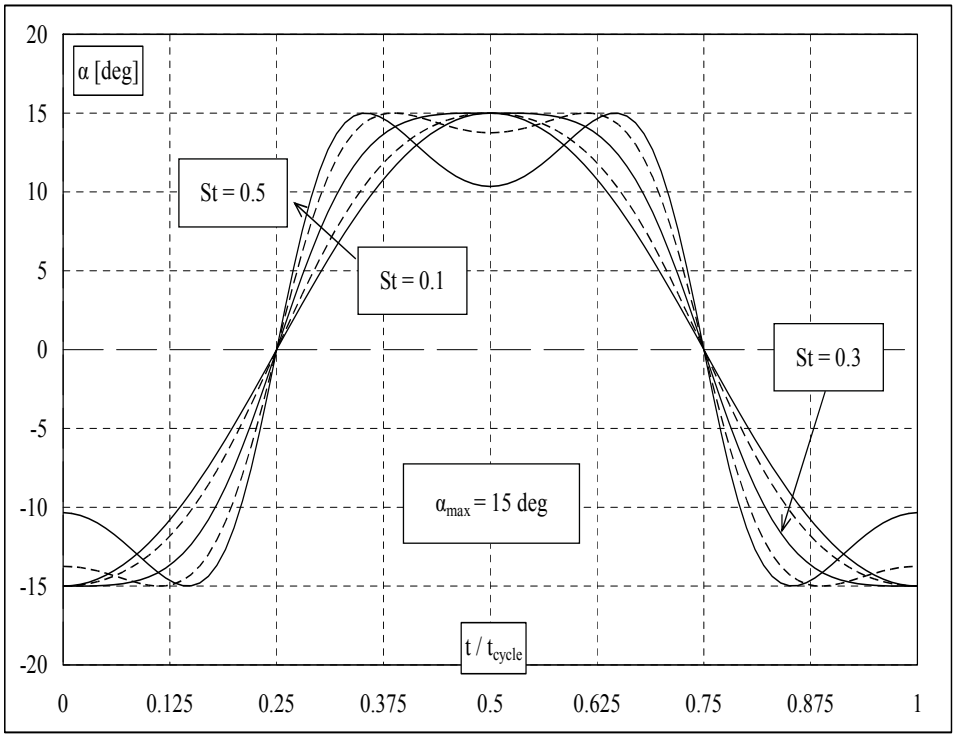

Figure 3: The instantaneous angle of attack is displayed as a function of St and time, where t_{cycle} is the duration in seconds of a complete oscillation of the wing.

Laplace's equation and Green's third identity. In the body-fixed coordinate system, at time t and for each wing collocation point it can be written as

$$\frac{1}{4\pi}\int_S \left[\sigma\left(\frac{1}{r}\right) - \mu\frac{\partial}{\partial n}\left(\frac{1}{r}\right)\right] dS - \frac{1}{4\pi}\int_{S_w} \mu_w \frac{\partial}{\partial n}\left(\frac{1}{r}\right) dS = 0, \tag{6}$$

where S and S_w indicate the wing and wake surface, respectively, and μ_w is the strength of the wake doublet distribution. To define uniquely the problem μ_w has to be known or related to the unknown doublets on S by the means of a suitable condition, that is, the Kutta condition. It is important to note that S_w changes with time, that is, new portions of the wake surface are added as the time advances. Besides, the wake shape has to be properly modelled.

The discretized form of Equation (6) can be written as

$$\sum_{j=1}^{N*N_S} C_j \mu_j + \sum_{j=1}^{N*N_S} B_j \sigma_j + \sum_{l=1}^{N_t} \sum_{k=1}^{N_S} C_{wl}^k \mu_{wl}^k = 0, \tag{7}$$

where N_t is the number of time steps. At each time step, N_S wake panels are shed, one for each wing strip. The number of wake panels is then equal to $N_t * N_S$. Each quadrilateral wake panel has an assigned chordwise length l_w and a constant strength doublet distribution μ_w on it. Moreover,

$$C_j = -\frac{1}{4\pi} \int_{S_j} \frac{\partial}{\partial n} \left(\frac{1}{r} \right) dS_j \tag{8}$$

and

$$B_j = \frac{1}{4\pi} \int_{S_j} \frac{1}{r} dS_j \tag{9}$$

are the appropriate three-dimensional doublet and source influence coefficients of panel j at the considered wing collocation point, respectively. They are only dependent on the wing and wake geometry, where r is the distance between the panel j and the respective collocation point and S_j the surface of panel j. More precisely, C_{wl}^k is defined as C_j, that is, r is the distance between the wake panel l and the respective wing collocation point and S_j the surface of the wake panel l, where the superscript k indicates the wake panel position along the span.

As previously stated, the wake has to be modelled. It was assumed that the wake panels remain where shed in the inertia coordinate system, that is, the wake follows the wing path. It has to be noted that, since the wing is moving, the position of the wake collocation points in the body-fixed coordinate system has to be calculated at each time step starting from their position in the inertia frame of reference. The body-fixed position of the wake panels closest to the trailing edge, i.e., those ones that are added at each time step, was set parallel to the chord. Besides, as discussed by Katz and Plotkin (2001), their length l_w was set proportional to the time step length Δt.

Equation (7) represents an algebraic system of $N * N_S$ equations but the unknowns are $N * N_S + N_S$ since at time t the doublet strengths of the previously shed wake panels are already derived. This means that, at each time step, N_S unsteady Kutta conditions at the wing trailing edge are needed to solve the system of equations. These conditions are derived from the unsteady Bernoulli equation that, following Cebeci et al. (2005), can be written at the trailing edge of the moving wing as

$$p_l + \frac{1}{2}\rho(q_l^2 - q_{kl}^2) + \rho \frac{\partial \phi_l^*}{\partial t} = p_u + \frac{1}{2}\rho(q_u^2 - q_{ku}^2) + \rho \frac{\partial \phi_u^*}{\partial t}, \tag{10}$$

where the subscripts l and u indicate the lower and upper surface of the trailing edge, respectively. At these points, a number of fluid properties are defined: p is the pressure, q the velocity, q_k the fluid kinematic velocity due to the motion of the wing and $\phi*$ the global potential function. The fluid velocity is the sum of q_k and the perturbation velocity, which is estimated by the means of the derivative of the perturbation potential over the wing, and ρ is the fluid density, which is assumed constant and uniform. Equation (10) can be rearranged as

$$\frac{2(p_u - p_l)}{\rho} = (q_l^2 - q_{kl}^2) - (q_u^2 - q_{ku}^2) - 2\frac{\partial(\phi_u^* - \phi_l^*)}{\partial t}. \tag{11}$$

The flow velocity and pressure difference are assumed finite at the trailing edge by imposing that the third term on the right hand side of Equation (11) there is also finite. This condition can be written as

$$\phi_u^* - \phi_l^* = (\phi_{\infty u} + \phi_u) - (\phi_{\infty l} + \phi_l) \quad = (\phi_{\infty u} - \mu_u) - (\phi_{\infty l} - \mu_l) = -\mu_w \tag{12}$$

or more concisely as

$$\mu_l - \mu_u + \mu_w = \phi_{\infty l} - \phi_{\infty u}. \tag{13}$$

It can be noted that -μ_w represents the instantaneous bound circulation Γ, i.e. the line integral of the fluid velocity around the considered strip. In other words, Γ is equivalent to the jump in the potential at the trailing edge.

Another possible unsteady Kutta condition (based on that developed by Bose, 1994) can involve more specifically the fluid velocities. If the pressure difference at the trailing edge is assumed null, Equation (11) becomes

$$(q_l^2 - q_{kl}^2) + 2\frac{\partial \phi_l^*}{\partial t} = (q_u^2 - q_{ku}^2) + 2\frac{\partial \phi_u^*}{\partial t}. \tag{14}$$

By using Equation (13) a linearized form of Equation (14) can be written to obtain such a condition, that is

$$-C_1\mu_{l+1} - C_3\mu_{u-1} + (C_1 + C_3)\mu_u - \left(C_1 - \frac{2}{\Delta t}\right)\mu_w = \frac{2}{\Delta t}(C_4 - C_2) - \left(C_1 - \frac{2}{\Delta t}\right)(\phi_{\infty l} - \phi_{\infty u}) \tag{15}$$

where $C_1 = (\frac{\phi_{l+1} - \phi_l}{d_l^2} + 2\frac{q_{tl}}{d_l})_{t-\Delta t}$, $C_2 = \phi_{\infty l_t} - (\phi_{\infty l} + \phi_l)_{t-\Delta t}$, $C_3 = (\frac{\phi_u - \phi_{u-1}}{d_u^2} + 2\frac{q_{tu}}{d_u})_{t-\Delta t}$ and $C_4 = \phi_{\infty u_t} - (\phi_{\infty u} + \phi_u)_{t-\Delta t}$. ϕ_i is the value of the local potential function at the

collocation point i. The panels of each strip are numbered clockwise, from the bottom of the trailing edge to the top. d_i indicates the distance between the two respective consecutive collocation points and q_{ti} is the component of the kinematic velocity tangential to panel i. t indicates the current time and Δt is the duration of each time step.

At the first time step it is not possible to use Equation (15). It can be replaced by another condition based on the trailing-edge fluid velocities. By using Equation (13) and assuming equal velocities the first time step trailing-edge condition is written as

$$-\frac{\mu_{l+1}}{d_l}-\frac{\mu_{u-1}}{d_u}+(\frac{1}{d_l}-\frac{1}{d_u})\mu_u-\frac{\mu_w}{d_l}=-q_{tl}-q_{tu}-\frac{\phi_{\infty l}-\phi_{\infty u}}{d_l}. \tag{16}$$

For the two-dimensional analysis Equation (13) was used as the unsteady Kutta condition at each time step and, as expected, a finite pressure difference was found at the trailing edge of the moving foil (La Mantia and Dabnichki, 2008).

In the three-dimensional computer program Equation (13) was replaced by Equations (15) and (16). The choice led to a steadier trailing-edge pressure difference as a function of time. To ensure a null pressure difference Equations (15) and (16) should be implemented in an iterative procedure (Bose, 1994) but there is not any strong experimental evidence that for unsteady motions of high frequency and large amplitude the pressure difference at the trailing edge has to be always null (La Mantia and Dabnichki, 2008).

The devised code, which assumes an incompressible and irrotational flow, can evaluate the global potential function, at each time step. It is then possible to calculate the velocities' distribution over the wing in the body-fixed coordinate system, which is moving together with the wing, by estimating the spatial derivative of the potential function over the wing. The subsequent calculation of the pressure coefficient is followed by the evaluation of the centre of pressure acceleration in the inertia frame of reference. This last one is later used for the forces coefficients calculations. A time-averaged force is obtained before computing the coefficients and the mass of the wing needed to be assumed. Following Read et at. (2003), a 0.6 m wing span s and a 300 kg/m^3 wing average density (which is the wood mean density) are chosen. The wing mass results then equal to roughly 0.15 kg, i.e. 1.47 N. The water density ρ, set at 1000 kg/m^3, is also used for the evaluation of the forces coefficients.

Following Cebeci et al. (2005), the pressure coefficient C_p at each wing collocation point and time step is defined as

$$C_p=\frac{p-p_\infty}{\frac{1}{2}\rho Q_\infty^2}=\frac{q_k^2}{Q_\infty^2}-\frac{q^2}{Q_\infty^2}-\frac{2}{Q_\infty^2}\frac{\partial\phi^*}{\partial t}. \tag{17}$$

The system of pressure forces acting on the wing can be represented by an equivalent single point force. This force should be applied at the centre of pressure, which is also defined as the point where the total moment is zero. The following equation is then used to evaluate the position of the centre of pressure (x_{cp}, z_{cp}) for each wing strip

$$C_m + C_{px} z_{cp} + C_{pz} x_{cp} = 0, \tag{18}$$

where C_m is the non-dimensional moment due to the pressure forces evaluated at the leading edge: it is positive if clockwise. C_{px} and C_{pz} are the non-dimensional pressure forces in the x and z directions of the body-fixed frame of reference, respectively. It is possible to assume that z_{cp} is null since the section thickness is much smaller than its chord and the position of the centre of pressure is evaluated as

$$x_{cp} = -\frac{C_m}{C_{pz}}. \tag{19}$$

Moreover, the centre of pressure is assumed to be in the middle of the considered wing strip, in the spanwise direction.

The time-averaged forces in the x and z directions of the inertia coordinate system are respectively defined as

$$\bar{F}_x = m_w a_{ref} a_x \tag{20}$$

and

$$\bar{F}_z = m_w a_{ref} a_z, \tag{21}$$

where m_w is the wing mass, a_x and a_z are the time-averaged non-dimensional centre of pressure accelerations in the inertia frame of reference and a_{ref} is then a reference acceleration defined as

$$a_{ref} = \frac{l_{ref}}{t_{ref}^2} = \frac{l_{ref}}{(\frac{l_{ref}}{Q_{ref}})^2} = \frac{c}{(\frac{c}{Q_\infty})^2} = \frac{Q_\infty^2}{c}, \tag{22}$$

where l_{ref}, t_{ref} and Q_{ref} are the reference length, time and velocity, respectively. Besides, c=0.1 m and Q_∞=0.4 m/s. The Reynolds number Re is then equal to 40,000, if the dynamic viscosity is set to 0.001 Pa•s, which is the water viscosity at 20 ˚C. The forces coefficients in the x and z directions of the inertia coordinate system, which are also called the thrust and lift coefficients, respectively, are defined as

$$C_{Fx} = \frac{\bar{F}_x}{\frac{1}{2}\rho c s Q_\infty^2} \tag{23}$$

and

$$C_{Fz} = \frac{\bar{F}_z}{\frac{1}{2}\rho c s Q_\infty^2}. \tag{24}$$

The thrust coefficient C_{Fx} is negative, if there is thrust, and the lift coefficient C_{Fz} is positive, if there is lift. It is important to underline that there are not forces acting in the span direction because the wing and imposed harmonic motion are symmetric.

3 Results and Discussion

A comparison with the computational results of a previously developed two-dimensional panel method (La Mantia and Dabnichki, 2008) was carried out. Two-dimensional (2D) and three-dimensional (3D) unsteady thrust are shown in Figure 4 as a function of time for a sample case (see Table 1 for the relevant motion parameters).

Ten complete loops and forty time steps for each cycle were used in both calculations. Two hundred linear panels model the NACA 0012 foil in the 2D computer program. The wing was then approximated by one section and two hundred quadrilateral panels in the corresponding three-dimensional procedure.

It can be seen that the forces patterns are very close, if the motion parameters are the same. The 2D thrust coefficient is equal to -0.536 and the three-dimensional C_{Fx}=-0.529. This means that the 3D thrust coefficient is just 1.1 % smaller than the two-dimensional one.

It has to be noted that four entire loops are displayed in the figure and the 2D Kutta condition, that is, Equation (13), was implemented in the three-dimensional computer program for this calculation. Moreover, the wake shape was imposed in both cases, that is, the wake follows the kinematic time path of the wing in the inertia frame of reference.

The 3D forces are slightly lower in magnitude than the two-dimensional ones. The 3D numerical procedure takes into account a wing of finite span weather the two-dimensional computer program assumes a wing of infinite span that is later imposed equal to a finite value to estimate the forces.

This result underlines the most relevant difference between the two codes, that is, the pressure behaviour over the wing span is not constant as assumed in the 2D model.

Figure 5 displays the thrust coefficient C_{Fx} as a function of the number of panels N of each wing section. It can be seen that the numerical convergence is reached quite rapidly as N increases, that is, the thrust coefficient for N=500 is just 1.6 % larger than C_{Fx} for N=50.

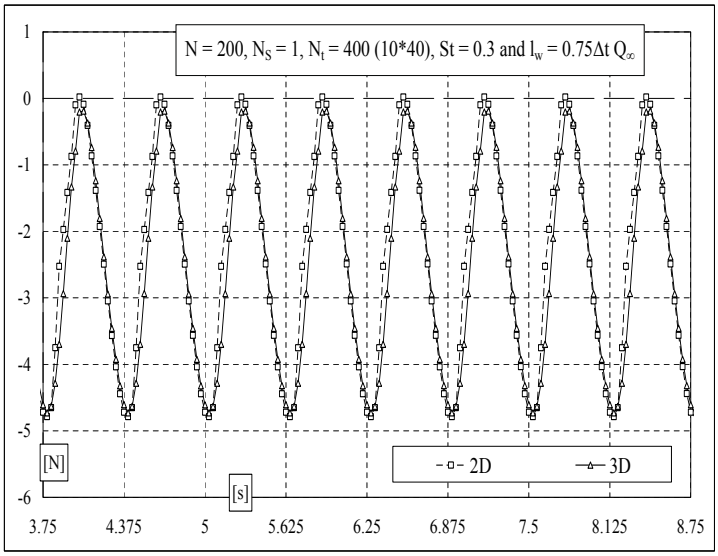

Figure 4: The instantaneous thrust is plotted as a function of time as estimated by the 2D (La Mantia and Dabnichki, 2008) and 3D codes. See also Table 1 for the relevant motion parameters.

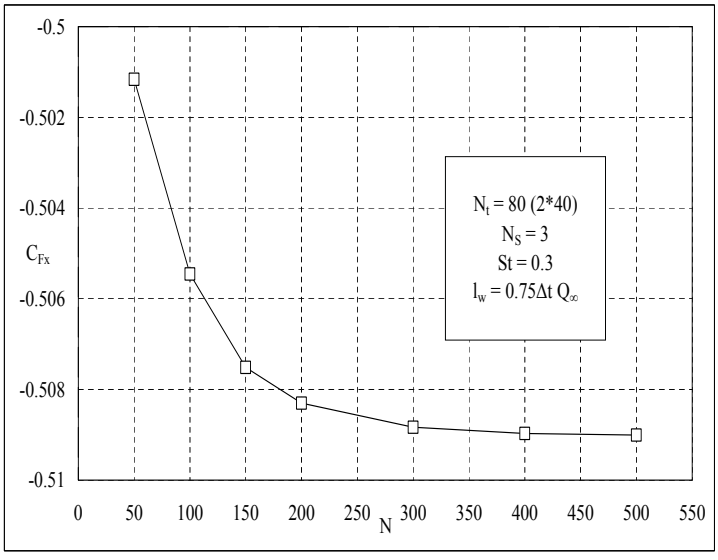

Figure 5: The thrust coefficient C_{Fx} is plotted as a function of the number of wing section panels N for St=0.3 and N_S=3. The number of cycles is two and forty time steps for each loop were used in the calculations. See also Table 1 for the relevant motion parameters.

In Figure 6 the pressure coefficient trend over the mid span section of the wing is displayed as a function of the collocation point position along the chord c, at the last time step and for two N. It can be noted that, as the number of panels for each section increases, the negative maximum of the pressure coefficient at the wing leading edge also increases. It is due to the more refined wing section model of the leading edge and can also explain the thrust coefficient behaviour as a function of N. See Figure 5 where the thrust coefficient sharply increases for N lower than 300.

In Figure 7 the thrust coefficient is plotted as a function of the number of wing section N_S. It can be seen that the wing span geometric model has a most relevant influence on the computational results than the wing section approximation. In other words, C_{Fx} for N_S=50 is 7.2 % smaller than the thrust coefficient for N_S=3. Besides, as N_S increases, the thrust coefficient decreases because the wing span model allows a more refined estimate of the pressure coefficient behaviour at the wing tips.

Figure 8 shows the maximum negative pressure coefficients as a function of the span position of the respective sections, at the last time step of the unsteady motion. They are placed at the leading edge of each section and their trend is related to the thrust coefficient behaviour as a function of N_S (see Figure 7). In other words, the pressure coefficient rise at the wing tips, which is a typical feature of three-dimensional analyses, can be easily spotted. It is related to the pressure difference between the two sides of the wing and leads to the formation of the well known wing-tip vortices.

The number of cycles does not have a significant impact on the results. For example, if ten loops (and fifty time steps for each cycle) are used in the calculation, the thrust coefficient for N_S=3 is just 0.8 % smaller than that of the two-cycles case displayed in Figure 7.

Fifty time steps for each cycle and two complete wing loops were then employed in the calculations presented in the next paragraphs, if it is not stated differently.

It has also to be noted that the wake shape was imposed in all three-dimensional calculations. The wake panels remain where shed and the wake then follows the imposed kinematic wing path.

Moreover, the wake length is fixed and equal to three quarter of the time step length Δt multiplied by the flow mean velocity Q_∞.

The relevant motion parameters used in the computations are summarized in Table 1. The Strouhal number, pitch amplitude and oscillation frequency are indicated by their respective range of values.

Figure 9 shows a typical two-cycles oscillating wing path in the (x, z) plane of the

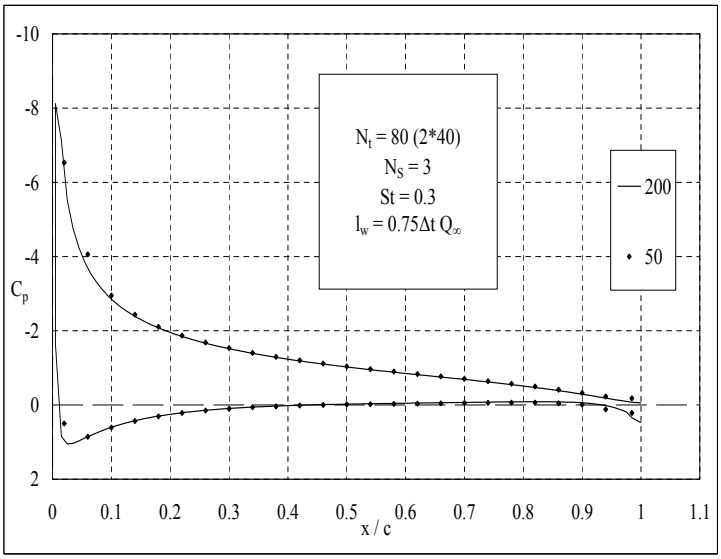

Figure 6: The pressure coefficients at the last time step are shown as a function of the collocation point position in the body-fixed coordinate system over the mid span section of the wing. The legend indicated the number N of panels for each section. See also Table 1 for the relevant motion parameters.

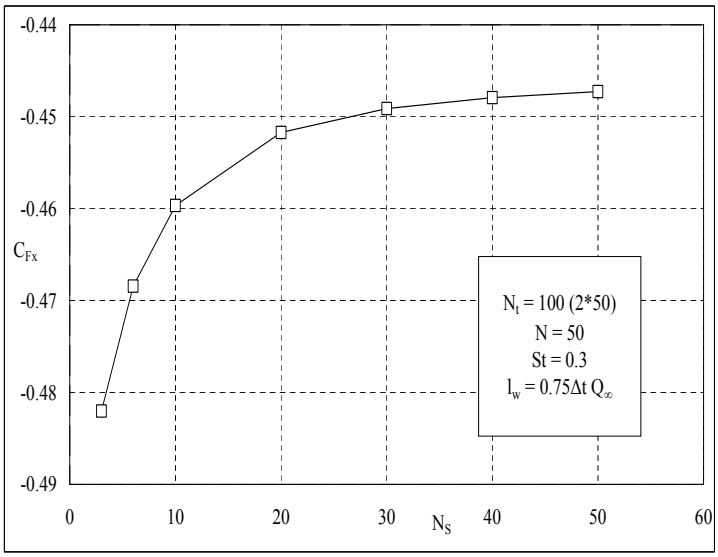

Figure 7: The thrust coefficient C_{Fx} is displayed as a function of the number of wing span panels N_S for St=0.3 and N=50. The number of cycles is two and fifty time steps for each loop were used in the calculations. See also Table 1 for the relevant motion parameters.

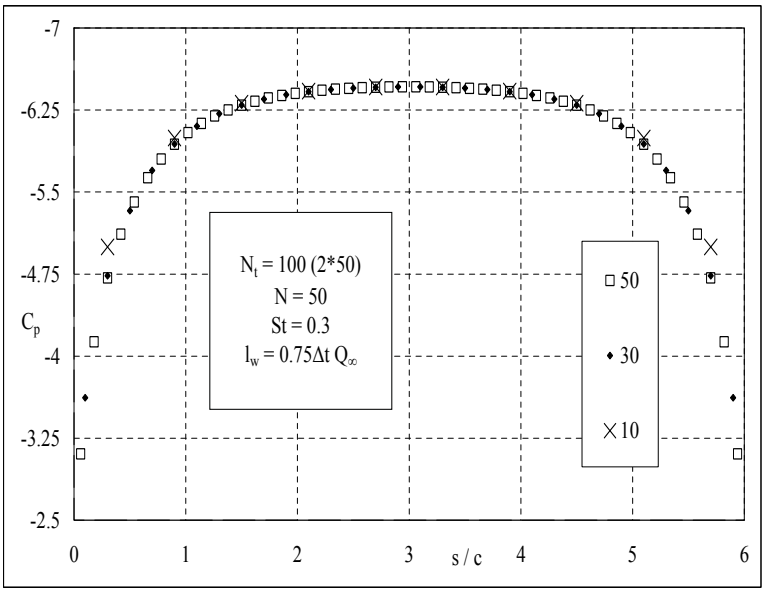

Figure 8: The maximum of the pressure coefficient C_p is plotted as a function of the wing section position along the span s in the body-fixed coordinate system. The legend indicated the number N_S of wing sections. See also Table 1 for the relevant motion parameters.

Table 1: List of the relevant parameters of the harmonic motions.

Chord c	0.1 m
Span s	0.6 m
Heave amplitude z_0	0.075 m
Pitch axis x_{pitch}	0.033 m
Maximum angle of attack α_{max}	15 deg
Phase angle ψ	90 deg
Q_∞	0.4 m/s
St	0.05 – 0.5
Pitch amplitude γ_0	-6.073 – 47.156 deg
Oscillation frequency ω	0.13 – 1.33 Hz
Re	40,000
Wing mass m_w	0.147 kg

inertia coordinate system that is the one perpendicular to the span.

The red line indicates the unsteady force time behaviour. It can be noted that, there is always thrust, i.e., the horizontal component of the displayed force is directed in the same direction of the wing forward motion. Besides, the time average of the force vertical component, i.e., the lift, is null, as expected for this kind of harmonic motion.

In Table 2 another comparison between two-dimensional and three-dimensional numerical results is carried out. As already noted, the 3D thrust coefficients are generally lower in magnitude than the two-dimensional ones. This is mainly due to the pressure behaviour over the wing span. The pressure coefficient negative maximum is placed at the wing mid span and, as already mentioned, C_p is not constant over the wing but becomes closer to zero at the wing tips.

Moreover, if the Strouhal number increases, the thrust coefficient becomes larger. In other words, the thrust produced by the flapping wing increases with the oscillation frequency in the rage of analyzed motions.

It is important to discuss the last two columns of Table 2. It can be seen that the trailing-edge pressure differences (at the last time step of the unsteady motion and at the wing mid span for the 3D analysis) are considerably steadier in the three-dimensional case, especially for *St* lower than 0.45. This result is mainly related to the three-dimensional formulation of the unsteady Kutta condition, that is Equations (15) and (16).

Table 2: The thrust coefficients and trailing-edge pressure differences are listed as a function of the Strouhal number *St* for two-dimensional (2D) and three-dimensional (3D) similar motions. See also Table 1 for the relevant motion parameters.

St	C_{Fx}		$\frac{C_{pl}-C_{pu}}{C_{p\max}}100$	
	2D	3D	2D	3D
0.05	-0.098	-0.054	2.72	2.52
0.10	-0.177	-0.122	3.71	2.22
0.15	-0.219	-0.187	4.77	2.18
0.20	-0.302	-0.258	5.41	2.46
0.25	-0.384	-0.343	5.95	2.89
0.30	-0.491	-0.447	6.28	3.29
0.35	-0.619	-0.566	6.70	3.82
0.40	-0.758	-0.696	7.85	5.08
0.45	-0.908	-0.835	10.17	7.75
0.50	-1.068	-0.981	14.43	13.25

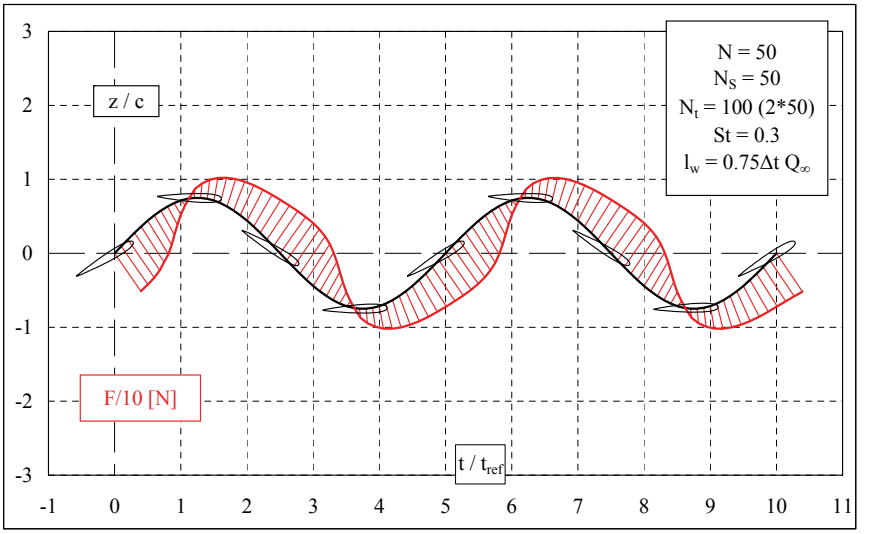

Figure 9: Wing path and force time trend are displayed in the inertia frame of reference for a sample case. The reference time t_{ref} is equal to 0.25 s. See also Table 1 for the relevant motion parameters.

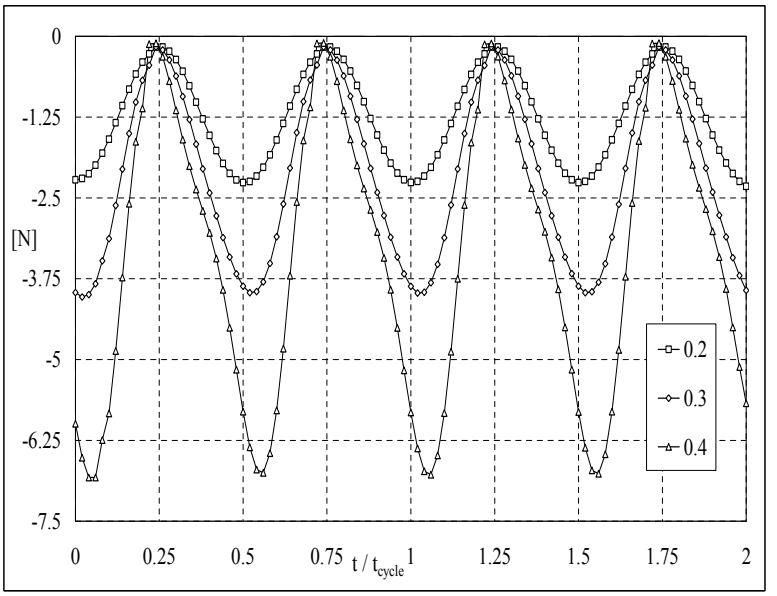

Figure 10: The instantaneous inertia thrust is plotted as a function of the normalized time for three Strouhal numbers. t_{cycle} is the time length of one entire wing cycle, that is, 1.875 s for St=0.2, 1.25 s for St=0.3 and 0.9375 s for St=0.4. See also Table 1 for the relevant motion parameters.

Figure 10 shows the thrust behaviour as a function of time in the inertia coordinate system for three different values of the Strouhal number. It can be noted that, as already mentioned, the force maximum increases with the oscillation frequency.

In Figure 11 the instantaneous inertia lift is shown as a function of time for the same situations displayed in Figure 10. It is important to remark that the time average value of the lift is null. Besides, the force trend is related to the corresponding angle of attack time path that depends on the imposed angle of attack maximum and Strouhal number. See Figure 3 where the instantaneous angle of attack is displayed as a function of St and time.

In Figure 12 comparisons with published experimental data (Read et al., 2003) and two-dimensional computational results (Garrick, 1936, and La Mantia and Dabnichki, 2008) are carried out. The thrust coefficient is plotted as a function of the Strouhal number.

The present three-dimensional computational results are much closer to the experimental data than the 2D ones. The wing finite span and consequently its tip vortices can be addressed as the main reason for the result.

Moreover, the agreement between experimental data and three-dimensional results is better at low Strouhal numbers, that is, low oscillation frequencies. This can be also attributed to the introduction in the numerical procedure of a more refined Kutta condition that lowers the trailing-edge pressure difference as a function of St (see Table 2).

The analytical results of the two-dimensional unsteady model of Garrick (1936) agree well with the two-dimensional computations (La Mantia and Dabnichki, 2008) for low Strouhal numbers, that is, for small oscillation amplitudes and frequencies. This is mainly due to the different Kutta condition that in the mathematical model of Garrick (1936) assumes a smooth flow at the foil trailing edge.

However, the discrepancy between experimental data and computational results can be more generally attributed to a number of different physical causes, such as wall interactions, flow separation for large instantaneous angle of attack and viscous drag, which are neglected in the potential model, as discussed by La Mantia and Dabnichki (2008).

Moreover, the added mass plays a significant role in defining the hydrodynamic forces acting on moving bodies, as shown by and Dabnichki (2006a). It is related to the body acceleration and can be intuitively defined as the mass of fluid moving with the body while the body is in motion. The movement of the surrounding water requires in fact an additional force over and above that necessary to accelerate the wing itself. The introduction of such inertia related effect in the procedure seems then to be a suitable option to better represent the experimental conditions. In the

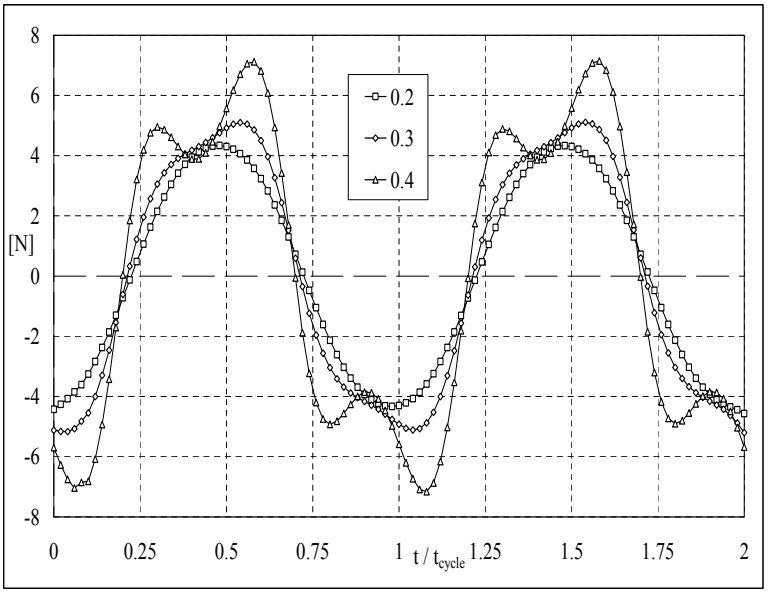

Figure 11: The instantaneous inertia lift is displayed as a function of time for the same cases illustrated in Figure 10. See also Table 1 for the relevant motion parameters.

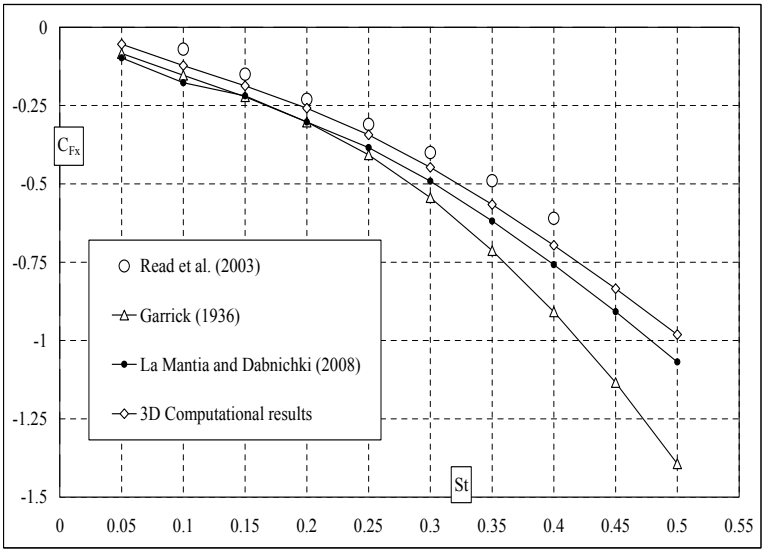

Figure 12: The thrust coefficient C_{Fx} is plotted as a function of the Strouhal number St. 'Read et al. (2003)' indicates experimental data. 'Garrick (1936)' and 'La Mantia and Dabnichki (2008)' denote computational results. The relevant motion parameters are c=0.1 m, s=0.6 m, x_{pitch}=0.033 m, Q_∞=0.4 m/s, z_0=0.075 m, ψ=90 deg and α_{max}=15 deg. Others are listed in Table 1.

same context, the buoyancy force that acts on the wing (and especially the moment that it generates) could also be taken into account. For example, if the wing is less dense than the fluid in which it is moving, another force will influence the unsteady motion. In other words, the numerical procedure assumed a neutrally buoyant body.

However, the disagreement between the computational results and experimental data is not a surprise and largely due to the differences between experimental models and conditions and the computer program potential flow assumptions.

4 Conclusions

A three-dimensional potential flow based boundary element method for evaluating the lift and thrust acting on wing oscillating in water was developed. Based on experimental evidence (Satyanarayana and Davis, 1978, Ho and Chen, 1981, and Poling and Telionis, 1986) and theoretical results (Young and Lai, 2004, Liebe, 2007) a novel formulation of the unsteady Kutta condition postulating finite pressure difference at the trailing edge of the moving wing was implemented. This formulation addresses an important need for a meaningful trailing-edge condition that reflects the physics of the unsteady problem.

Moreover, the Kutta condition was not sufficient to ensure unique solution for the unsteady problem. Additional assumptions such as the wake model and centre of pressure position needed to be added to in effect represent initial conditions for this dynamic problem.

The effects of tip vortices on the pressure distribution over the wing and the new trailing-edge condition can explain the closer agreement between the three-dimensional numerical results and experimental data (Read et al., 2003), if compared to the two-dimensional ones (Garrick, 1936, and La Mantia and Dabnichki, 2008).

An improved version of the three-dimensional code is being developed to asses the influence of added mass and viscous drag on the forces' estimate. As shown by Gardano and Dabnichki (2006a) this effect is essential in understanding the propulsion effect. However its importance for man-made structures lies in the accurate estimate of the strength requirements as discussed by Dabnichki and La Mantia (2007) and the developed method facilitates such comprehensive analysis.

References

Anderson, J.M.; Streitlien, K.; Barrett, D.S.; Triantafyllou, M.S. (1998): Oscillating Foils of High Propulsive Efficiency, *Journal of Fluid Mechanics*, Vol. 360, No. 1, 41-72.

Basu, B.C.; Hancock, G.J. (1978): The Unsteady Motion of a Two-Dimensional

Aerofoil in Incompressible Inviscid Flow, *Journal of Fluid Mechanics*, Vol. 87, No. 1, 159-178.

Bose, N. (1994): Explicit Kutta Condition for an Unsteady Two-Dimensional Constant Potential Panel Method, *AIAA Journal*, Vol. 32, No. 5, 1078-1080.

Cebeci, T.; Platzer, M.; Chen, H.; Chang, K.-C.; Shao, J. P. (2005): *Analysis of Low-Speed Unsteady Airfoil Flows*, Springer.

Chaplygin, S.A. (1910): On the Pressure Exerted by a Plane-Parallel Flow upon an Obstructing Body (Aeroplane Theory) (in Russian), *Mathematical Collections of Moscow*, Vol. 28, No.1, 120-166.

Dabnichki, P.; La Mantia, M. (2007): Dynamic loads and strength requirements for flapping wing. *Key Engineering Materials,* 348-49, 945-948.

Gardano, P.; Dabnichki, P. (2006a): Application of Boundary Element Method to Modelling of Added Mass and its Effect on Hydrodynamic Forces, *CMES: Computer Modeling in Engineering and Sciences*, Vol. 15, No. 2, 87-98.

Gardano, P.; Dabnichki, P. (2006b): On hydrodynamics of drag and lift of the human arm. *Journal of Biomechanics*, 39, 2767-2773.

Garrick, I.E. (1936): Propulsion of a Flapping and Oscillating Airfoil, NACA Report No. 567.

Hess, J.L. (1990): Panel Methods in Computational Fluid Dynamics, *Annual Review of Fluid Mechanics*, Vol. 22, 255-274.

Ho, C.-M.; Chen, S.-H. (1981): Unsteady Kutta Condition of a Plunging Airfoil, *Unsteady Turbulent Shear Flows* (Edited by Michel, R., Cousteix, J.; Houdeville, R.), Springer, 197-206.

Katz, J.; Plotkin, A. (2001): *Low-Speed Aerodynamics – Second Edition*, Cambridge University Press.

Kutta, W.M. (1910): Über eine mit den Grundlagen des Flugproblems in Beziehung stehende zweidimensionale Strömung, *Sitzungsberichte der Königlich Bayerischen Akademie der Wissenschaften*, Vol. 40, 1-58.

La Mantia, M.; Dabnichki, P. (2006): Unsteady Panel Method for Oscillating Foils, Advances in BE Techniques VII, 91-96.

La Mantia, M.; Dabnichki, P. (2007): High order velocity approximation for a flapping foil. Advances in BE Techniques VIII, 251-256.

La Mantia, M.; Dabnichki, P. (2008): Unsteady Panel Method for Flapping Foil, *Engineering Analysis with Boundary Elements*, `http://dx.doi.org/10.1016/j.enganabound.2008.08.001`.

Lauder, M.A.; Dabnichki P. (2005) Estimating propulsive forces - sink or swim?

Journal of Biomechanics, 38, 1984-1990.

Lauder M.A.; Dabnichki P.; Bartlett R.M. (2001) Improved accuracy and reliability of sweepback angle, pitch angle and hand velocity calculations in swimming, *Journal of Biomechanics*, 34, 31-39.

Liebe, R. (2007): Unsteady Flow Mechanisms on Airfoils: The Extended Finite Vortex Model with Applications, *Flow Phenomena in Nature – Volume 1: A Challenge to Engineering Design* (Edited by Liebe, R.), WIT Press, 283-339.

McCroskey, W.J. (1982): Unsteady Airfoils, *Annual Review of Fluid Mechanics*, Vol. 14, 285-311.

Poling, D.R.; Telionis, D.P. (1986): The Response of Airfoils to Periodic Disturbances – The Unsteady Kutta Condition, *AIAA Journal*, Vol.24, No. 2, 193-199.

Read, D.A.; Hover, F.S.; Triantafyllou, M.S. (2003): Forces on Oscillating Foils for Propulsion and Maneuvering, *Journal of Fluids and Structures*, Vol. 17, No. 1, 163-183.

Rozhdestvensky, K.V.; Ryzhov V.A. (2003): Aerohydrodynamics of Flapping-Wing Propulsors, *Progress in Aerospace Science*, Vol. 39, No. 8, 585-633.

Satyanarayana, B.; Davis, S. (1978): Experimental Studies of Unsteady Trailing-Edge Conditions, *AIAA Journal*, Vol. 16, No.2, 125-129.

Schouveiler, L.; Hover, F. S.; Triantafyllou, M.S. (2005): Performance of Flapping Foil Propulsion, *Journal of Fluids and Structures*, Vol. 20, No. 7, 949-959.

Sellier, A. (2008): Slow Viscous Motion of a Solid Particle in a Spherical Cavity, *CMES: Computer Modeling in Engineering and Sciences*, Vol. 25, No. 3, 165-179.

Sellountos, E.J.; Sequeira, A. (2008): A Hybrid Multi-Region BEM/LBIE-RBF Velocity-Vorticity Scheme for the Two-Dimensional Navier-Stokes Equations, *CMES: Computer Modeling in Engineering and Sciences*, Vol. 23, No. 2, 127-147.

Soares, D.; Mansur, W.J. (2005): An Efficient Time-Domain BEM/FEM Coupling for Acoustic-Elastodynamic Interaction Problems, *CMES: Computer Modeling in Engineering and Sciences*, Vol. 8, No. 2, 153-164.

Triantafyllou, M.S.; Techet, A.H.; Hover, F.S. (2004): Review of Experimental Work in Biomimetic Foils, *IEEE Journal of Oceanic Engineering*, Vol. 29, No. 3, 585-594.

Young, J.; Lai, J.C.S. (2004): Oscillation Frequency and Amplitude Effects on the Wake of a Plunging Airfoil, *AIAA Journal*, Vol. 42, No. 10, 2042-2052.

Zhukovski, N.E. (1910): Über die Konturen der Tragflächen der Drachenflieger, *Zeitschrift für Flugtechnik und Motorluftschiffahrt*, Vol. 1, 281-284.